Improved Signal Processing Techniques for the Analysis of High Resolution Serosal Slow Wave Activity in the Stomach

Niranchan Paskaranandavadivel, Leo K. Cheng, Peng Du, Gregory O'Grady, Andrew J. Pullan

Abstract— High resolution electrical mapping of slow waves on the stomach serosa has improved our understanding of gastric electrical activity in normal and diseased states. In order to assess the signals acquired from high resolution mapping, a robust framework is required. Our framework is semi-automated and allows for rapid processing, analysis and interpretation of slow waves via qualitative and quantitative measures including isochronal activation time mapping, and velocity and amplitude mapping. Noise removal techniques were validated for raw recorded signals, where three filters were evaluated for baseline drift removal and three filters for removal of high frequency interference. For baseline drift removal, the Gaussian moving median filter was most effective, while for eliminating high frequency interference the Savitzky Golay filter was the most effective. Methods for assessing slow wave velocity and amplitude were investigated. To estimate slow wave velocity, a finite difference approach with interpolation and smoothing was used. To evaluate the slow wave amplitude and width, a peak and trough method based on Savitzky Golay derivative filters was used. Together, these methods constitute a significantly improved framework for analyzing gastric high resolution mapping data.

I. INTRODUCTION

The motility of the stomach is governed by an underlying rhythmic electrical activity, termed the slow wave (SW). In the normal human these slow waves (SWs) occur at three cycles per minute (cpm) and are generated and propagated by the interstitial cells of Cajal (ICC), which are coupled to smooth muscle cells [1].

Traditionally sparse electrodes were used to record SWs, and frequency analysis was mainly performed but propagation patterns could not be accurately determined [2]. With the development of high resolution (HR) techniques in gastric SW mapping (up to 256 channels of simultaneous recording) [3], manual analysis of the data has been common practice [4]. 'SmoothMap' is a software which was developed for HR mapping purposes which uses a manual method for marking and analysis of gastrointestinal signals [5]. This software currently only allows for sequential wave analysis, and does not have any noise removal filters. Due to the large number of signals that needed to be processed and

analyzed from HR gastric SW mapping, a significant amount of time was spent manually marking and clustering SWs and thereafter sequentially calculating amplitudes and velocities of SWs. This method of manual analysis is time consuming, labour intensive and is an ineffective approach if a number of subject recordings are to be made, thus limiting the progress in the field. Effective methods for visualization of isochronal time maps, velocity and amplitude fields were also lacking. To this end we have developed a semi-automated framework and related processing techniques for analyzing and interpreting HR gastric SWs.

The framework for analyzing HR gastric SWs is shown in Fig. 1, where the raw data was first downsampled after which the prevailing baseline and high frequency noise was removed. The SWs were then automatically detected using a variable threshold algorithm [6], and clustered into their propagating waves using a polynomial based region growing method [7]. Detection and clustering of SWs were then visually assessed and manually corrected if necessary. The velocity of the propagating SWs and their signal amplitudes were then computed and visualized along with the isochronal activation time maps. The methods for detection and clustering of the SWs have been described in detail in [6] and [7]. Here we describe the noise present in the signals along with validation of noise removal techniques on realistic synthetic gastric SWs. This is followed by a description of improved methods for estimating velocity of propagating SWs and its signal amplitude and width.

II. NOISE REMOVAL

During bio-electrical recordings, noise is ubiquitous and is recorded along with the signals of interest. The noise inherent in HR gastric serosal recordings has been classified as a combination of baseline drift and high frequency interference. The baseline drift may be due to the alternating electrode-serosa impedance and body movements. The high frequency interference may be generated by the ventilator, other electronic systems, and possibly the electrical or mechanical activity of the heart or both. Unlike the electrocardiology field, where there are standards about the use of filter settings from professional societies [8], there are no recommended filter settings for use in gastrointestinal electrical recordings.

To eliminate the baseline drift in the signals, three filters were evaluated; High pass Butterworth filter, Gaussian moving median filter [9], and Discrete Wavelet filter [10]. To eliminate high frequency interference in the signals, three filters were evaluated; Low pass Butterworth filter; Savitzky Golay filter [11], and Discrete Wavelet filter using a soft
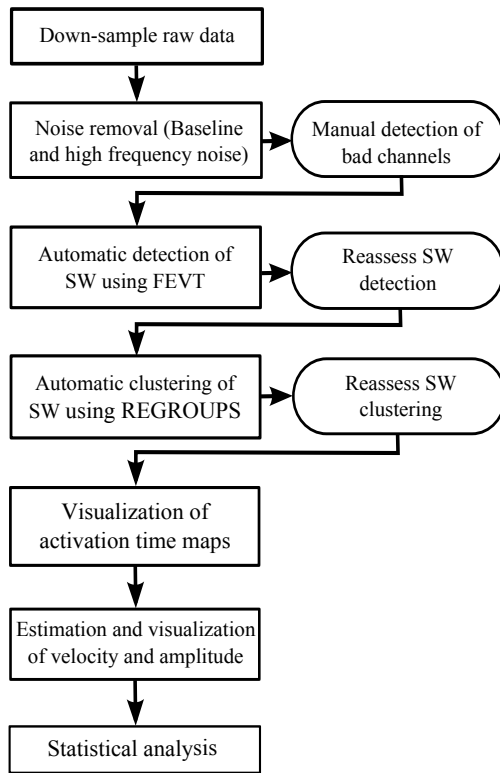
Fig. 1. Methods used to analyze gastric serosal electrical recordings. FEVT stands for falling edge variable threshold, and it is the algorithm used to detect slow wave (SW) events. REGROUPS stands for a region growing procedure and uses a polynomial surface estimate to cluster SW events into SW cycles.

Filter type: Baseline drift	Parameters
High Pass Butterworth filter	Filter Order: 2, Cutt Off: 1 cpm
Gaussian moving median filter [9]	Window width: 20 seconds
Discrete Wavelet filter [10]	Wavelet: Symlet, Decomposition level: 11
Filter type: High Frequency	**Parameters**
Low Pass Butterworth filter	Filter Order: 2, Cutt Off: 60 cpm
Savitzky Golay (SG) filter [11]	Polynomial order: 9, Window width - 1.7 seconds
Discrete Wavelet filter [12]	Wavelet: Symlet, Soft threshold: BayesShrink

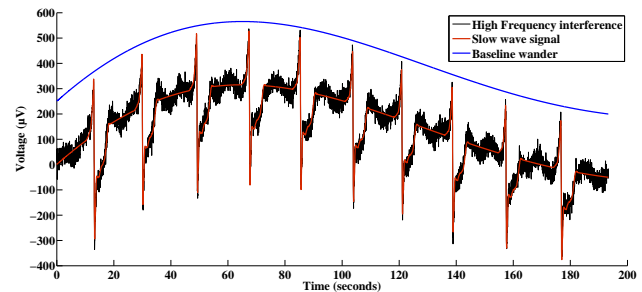TABLE I

NOISE REMOVAL TECHNIQUES, AND SPECIFICATIONS.

Fig. 2. Synthetic slow wave porcine signal with artificial baseline wander and high frequency noise.

threshold [12]. These filters were chosen based on reported effectiveness and computational efficiency. The parameters for the filters (as shown in Table I) were chosen based on the fundamental and harmonic frequencies of SWs.

A. Validation of filters with synthetic signals

To evaluate the effectiveness of the chosen filters, realistic synthetic signals were created from experimental signals. To include various morphologies of the SWs, fifteen signals were created from three representative porcine serosal gastric recordings. Five electrode signals were then chosen from each of these sets, with a time period ranging from three to ten minutes. For each of the electrodes, the SWs were detected [6], and stacked. An average SW morphology for each electrode was then defined by the first principal component from the singular value decomposition of the stacked SWs [13]. The morphology was amplitude scaled and placed into its original position on an uniform vector. Artificial baseline and high frequency noise in sinusoidal form were added to the synthetic signals to represent raw experimental recordings, as seen in Fig. 2. The following measures were used to test for the effectiveness of the filters,

$$\text{Baseline Correction Ratio (BCR)} = \frac{\|b_o - b_e\|_2}{\|b_o\|_2} \quad (1)$$

$$\text{Noise Correction Ratio (NCR)} = \frac{\|n_o - n_e\|_2}{\|n_o\|_2} \quad (2)$$

$$\text{Signal Distortion Ratio (SDR)} = \frac{\|s_o - s_e\|_2}{\|s_o\|_2} \quad (3)$$

where b_o is the artificial baseline, b_e is the estimated baseline, n_o is the artificial noise, n_e is the estimated noise, s_o is the synthetic signal, s_e is the signal after application of the filter, and $\|\cdot\|_2$ is the Euclidean norm. Ideally BCR, NCR and SDR will be 0.

1) Synthetic Test Case Results: Effective noise removal techniques are required in order to reveal the SW morphology without significant distortion. This step is critical because a clean signal will yield a better detection rate of SWs [6]. From the results (as shaded in Table II), to eliminate

Baseline	HP Butterworth	Median [9]	Wavelet [10]
BCR	1.99	0.0016	0.012
HF Noise	LP Butterworth	Savitzky Golay [11]	Wavelet [12]
NCR	0.80	0.78	0.92
SDR	0.23	0.17	0.48

TABLE II

NOISE REMOVAL RESULTS. HP IS HIGH PASS, LP IS LOW PASS, HF IS HIGH FREQUENCY INTERFERENCE, WHILE BCR IS THE BASELINE CORRECTION RATIO, NCR IS THE NOISE CORRECTION RATIO, AND SDR IS THE SIGNAL DISTORTION RATIO.

baseline wander, the Gaussian moving median filter was most suitable, and for high frequency noise removal, the Savitzky Golay (SG) filter was most suitable.

III. VELOCITY ESTIMATION

Once the noise has been eliminated from the raw signal, the fiducial point of the SWs can be detected and clustered to form an isochronal time map [7]. Velocity fields can be constructed from these time maps, to provide a quantitative measure of the underlying SW activity in the stomach.

The definition of velocity in two dimensions is as follows,

$$\begin{bmatrix} V_x \\ V_y \end{bmatrix} = \begin{bmatrix} \frac{T_x}{T_x^2 + T_y^2} \\ \frac{T_x}{T_x^2 + T_y^2} \end{bmatrix} \quad (4)$$

where $T_x = \partial T / \partial x$ and $T_y = \partial T / \partial y$ are the gradients of the isochronal time map with respect to the x and y directions. The simplest approach to estimate velocity is to take the finite difference (one sided difference for the edges and central difference for the internal array) of the time map. This finite difference approach is used by the 'SmoothMap' software and has been applied in several studies [14], [3], however it has two main disadvantages. First, any noise in the activation time map would be amplified by the finite difference process, and secondly regions of missing data will increase the area where velocity cannot be estimated. Noise can be present in the time maps due to misalignment of recording arrays or incorrect fiducial detection or clustering of SWs. Regions of missing data may be due to electrodes not being in contact with the serosa or the underlying serosa being non-conductive and having no SW activity.

To circumvent these problems a finite difference approach with interpolation and smoothing is introduced. After applying a finite difference approach, the edges of the grid were padded by two electrodes, and all of the values were interpolated using an inverse distance squared interpolation as in 5 [15],

$$Y = \frac{\sum_{i=1}^n \frac{X_i}{D_i^2}}{\sum_{i=1}^n \frac{1}{D_i^2}} \quad (5)$$

where Y is the unknown value to be interpolated, X_i is the known value at point i, D_i is distance between the known and unknown value, and n is the number of the known values in the grid. V_x and V_y were then smoothed using a Gaussian filter (defined in (6)), to reduce any noise amplification by the finite difference approach, after which the vectors were normalized for plotting.

$$G_{filt}(x, y) = e^{\frac{\hat{x}^2 + \hat{y}^2}{2\sigma}} \quad (6)$$

In (6), G_{filt} is the Gaussian filter, $\hat{x}$ and $\hat{y}$ defines the size of the filter and σ is the standard deviation of the filter. The values for the Gaussian filter were empirically chosen to be as $\hat{x} = \hat{y} = 1 - 5$ in steps of 1 and σ as 0.75.

Fig. 3 shows the velocity field of an isochronal SW propagation map, where the velocity was estimated using the finite difference method with interpolation and smoothing. The corresponding amplitude map of the SWs is also shown.
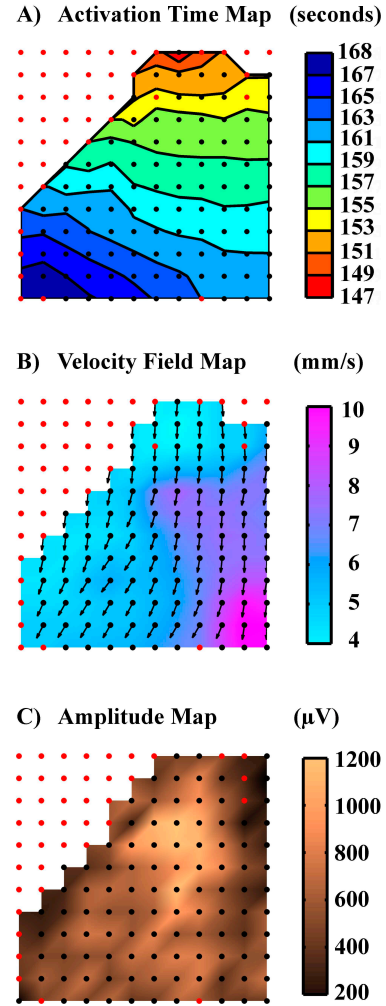

Fig. 3. Propagation of porcine gastric slow wave A) isochronal activation time map and its B) associated velocity and C) amplitude field map. The velocity fields were computed using a finite difference method with interpolation and smoothing and displayed as a velocity map, with arrows showing propagation direction. Amplitude of slow waves at the activation times were calculated using a peak and trough method. The red dots denote electrodes that did not yield any information in the particular wave, while the black dots are electrodes that detected an activation time. The data for which red circles are plotted were interpolated using an inverse distance squared interpolation with a radius of two electrodes.

IV. AMPLITUDE ESTIMATION

The amplitude of the SW was estimated as the difference in peak and trough values of the event. A simple method to calculate amplitude would be to place a window around the fiducial point of the SW and take the maximum and minimum values of the window. This method is used by the 'SmoothMap' software to estimate SW amplitude. The assumption with this method is that the signal is noise free. In experimental recording, this is not always the case, as SWs are superimposed on noise or have physiological electrogram fractionation [4].

In order to allow for precise detection of the peak and trough of the SW, the derivatives of the signal were computed to detect the maxima, minima, and inflection points. Fig. 4 shows the use of the first derivative of the signal, where
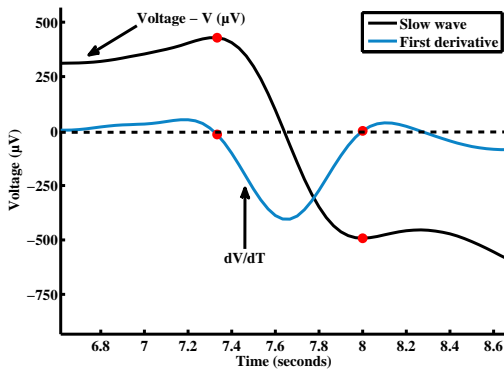
Fig. 4. Amplitude estimation via a peak and trough method. The peaks and troughs are found using the zero crossing of the first and second derivative. Here the first derivative (dV/dT) is shown along with the slow wave. The zero crossing position (marked in red dots) of the first derivative corresponded to the peak and trough on the slow wave. The closest zero crossing position to the slow wave fiducial point was chosen as the peak and trough position of the slow wave.

its zero crossing positions corresponding to the peak and trough position on the slow wave signal. Due to the existence of noise in the signal, the SWs were differentiated using SG derivative filters, to moderate noise amplification in the derivative of the signal [16]. The derivative of the signal becomes smoother when the length of the SG derivative filters is increased or by decreasing the polynomial order and vice versa. The zeros crossings of the first and second derivative were found, and the closest point to the fiducial SW was chosen as the peak and trough positions of the event. The SW width and amplitude was subsequently computed.

V. CONCLUSION

We have presented improved signal processing techniques to process and analyze high resolution recordings of gastric slow waves. Noise removal is an essential step in data analysis of bio-electrical activity, and the filters applied have been validated against realistic slow wave synthetic signals to give confidence for use in experimental signals. Qualitative and quantitative measures of slow wave activity are then computed using automated methods for interpretation of the underlying electrical activity in the stomach.

To eliminate noise in the signals, a Gaussian moving median filter was used to estimate and remove the baseline drift, and a Savitzky Golay filter was used to eliminate the high frequency interference. The accuracy of the velocity and amplitude estimation greatly depended on the noise levels present in the signals and the precise alignment of electrode arrays. To calculate velocity, the finite difference approach was interpolated and smoothed to moderate the noise level present in the recorded signals and electrode array. In order to calculate the amplitude and width of slow waves a Savitzky Golay derivative method was employed to find the peaks and troughs of the bio-electrical event.

The assumption with the velocity estimation procedure was that the recording electrode array was a regular grid.

Other methods such as polynomial fitting may be needed if the spatial configuration of the recording electrode array is irregular [17].

The methods and processing techniques described here are for the analysis of serosal gastric slow wave signals. Nonetheless, this approach can be adapted for other gastrointestinal signals, such as in high resolution intestinal electrical recordings.

REFERENCES

[1] L. K. Cheng, G. O'Grady, P. Du, J. U. Egbuji, J. A. Windsor, and A. J. Pullan, "Gastrointestinal system," *Wiley Interdiscip. Rev. Syst. Biol. Med.*, vol. 2, no. 1, pp. 65–79, 2010.

[2] G. O'Grady, P. Du, W. J. E. P. Lammers, J. U. Egbuji, P. Mithraratne, J. D. Z. Chen, L. K. Cheng, J. A. Windsor, and A. J. Pullan, "High-resolution entrainment mapping of gastric pacing: a new analytical tool," *Am. J. Physiol. Gastrointest. Liver Physiol.*, vol. 298, no. 2, p. G314, 2010.

[3] P. Du, G. O'Grady, J. U. Egbuji, W. J. E. P. Lammers, D. Budgett, P. Nielsen, J. A. Windsor, A. J. Pullan, and L. K. Cheng, "High-resolution mapping of in vivo gastrointestinal slow wave activity using flexible printed circuit board electrodes: methodology and validation," *Ann. Biomed. Eng.*, vol. 37, no. 4, pp. 839–846, 2009.

[4] G. O'Grady, P. Du, L. K. Cheng, J. U. Egbuji, W. J. E. P. Lammers, J. A. Windsor, and A. J. Pullan, "Origin and propagation of human gastric slow-wave activity defined by high-resolution mapping," *Am. J. Physiol. Gastrointest. Liver Physiol.*, vol. 299, no. 3, p. G585, 2010.

[5] W. J. E. P. Lammers. (2011) Smoothmap v3.03. [Online]. Available: http://www.fmhs.uaeu.ac.ae/smoothmap/

[6] J. C. Erickson, G. O'Grady, P. Du, C. Obioha, W. Qiao, W. O. Richards, L. A. Bradshaw, A. J. Pullan, and L. K. Cheng, "Falling-Edge, Variable Threshold (FEVT) Method for the Automated Detection of Gastric Slow Wave Events in High-Resolution Serosal Electrode Recordings," *Ann. Biomed. Eng.*, vol. 38, no. 4, pp. 1511–1529, 2010.

[7] J. C. Erickson, G. O'Grady, P. Du, J. U. Egbuji, A. J. Pullan, and L. K. Cheng, "Automated Gastric Slow Wave Cycle Partitioning and Visualization for High-resolution Activation Time Maps," *Ann. Biomed. Eng.*, pp. 1–15, 2011.

[8] P. Kligfield, L. S. Gettes, J. J. Bailey, *et al.*, "Recommendations for the standardization and interpretation of the electrocardiogram:: Part i: The electrocardiogram and its technology: A scientific statement from the american heart association electrocardiography and arrhythmias committee, council on clinical cardiology; the american college of cardiology foundation; and the heart rhythm society. endorsed by the international society for computerized electrocardiology," *Heart Rhythm*, vol. 4, no. 3, pp. 394–412, 2007.

[9] M. S. Friedrichs, "A model-free algorithm for the removal of baseline artifacts," *J. Biomol. NMR.*, vol. 5, no. 2, pp. 147–153, 1995.

[10] D. Zhang, "Wavelet approach for ecg baseline wander correction and noise reduction," in *Proc. IEEE EMBS 27th Annual Conf.*, Shangai, China, pp. 1212–1215, 2005.

[11] S. Hargittai, "Savitzky-Golay least-squares polynomial filters in ECG signal processing," in *Comput. Cardiol.*, 2005, pp. 763–766.

[12] S. G. Chang, B. Yu, and M. Vetterli, "Adaptive wavelet thresholding for image denoising and compression," *IEEE Trans. Image Processing*, vol. 9, no. 9, pp. 1532 –1546, Sept. 2000.

[13] R. Alcaraz and J. J. Rieta, "Adaptive singular value cancelation of ventricular activity in single-lead atrial fibrillation electrocardiograms," *Physiol. Meas.*, vol. 29, p. 1351, 2008.

[14] W. J. E. P. Lammers, L. V. Donck, J. A. J. Schuurkes, and B. Stephen, "Peripheral pacemakers and patterns of slow wave propagation in the canine small intestine in vivo," *Can. J. Physiol. Pharmacol.*, vol. 83, no. 11, pp. 1031–1043, 2005.

[15] E. H. Isaak and R. M. Srivastava, *An Introduction to Applied Geostatistics*. Oxford University Press, New York, 1989.

[16] R. King, C. Ruffin, F. LaMastus, and D. Shaw, "The analysis of hyperspectral data using Savitzky-Golay filtering-Practical issues (Part 2)," *Proc. IEEE IGARSS*, 1999.

[17] P. V. Bayly, B. H. KenKnight, J. M. Rogers, R. E. Hillsley, R. E. Ideker, and W. M. Smith, "Estimation of conduction velocity vector fields from epicardial mapping data," *IEEE Trans. Biomed. Eng.*, vol. 45, no. 5, pp. 563 –571, May 1998.